Influences of the Non-Covalent Interaction Strength on Reaching High Solid-State Order and Device Performance of a Low Bandgap Polymer with Axisymmetrical Structural Units

Jyun-Fong Jheng, Yu-Ying Lai, Jhong-Sian Wu, Yi-Hsiang Chao, Chien-Lung Wang, and Chain-Shu Hsu**

Conjugated polymers consisting of an alternating arrangement of an electron-rich donor (D) unit and an electron-deficient acceptor (A) unit have been recognized as high-performance materials used in optoelectronic applications, such as organic photovoltaics (OPV) and organic field-effect transistors (OFETs).[1] Abundant low band-gap (LBG) polymers have been created via modifications in the D and A units to facilitate the fine-tuning of the frontier orbitals of these polymers. Proper D-A combinations provided LBG polymers good light-harvesting ability, optimized highest occupied molecular orbital level (E_{HOMO}) for high open circuit voltage (V_{oc}), and appropriate lowest unoccupied molecular orbital level (E_{LUMO}) for efficient charge-carrier generation, which requires sufficient E_{LUMO} offset between the *p*-type LBG polymers and the *n*-type fullerene-based acceptors.[2] Currently, bulk-heterojunction (BHJ) polymer solar cells (PSCs) using LBG polymers with prudent molecular design have reached power conversion efficiencies (PCEs) around 7%,[3] and even higher PCEs have been achieved with improved device architectures and via interfacial layer modifications.[4] In the OFET applications, conjugated polymers with alternating D-A arrangement also demonstrate high mobilities and air stabilities because of their closer π–π stacking distances and lower-lying E_{HOMO}s.[5]

While chemical structures of the polymers determine the intrinsic optoelectronic properties of the polymers, the non-covalent intermolecular interactions govern the self-assembly processes[6] and the formation of solid-state structures, which act as a determinative factor on the macroscopic device performances.[7] Although wide varieties of D-A combinations have proven their effectiveness in improving devices performances,[8] the effects of these novel structure units in the non-covalent interactions and phase structures of the LBG polymers were less explored. Takimiya et al. and Pei et al. pointed out the importance of the symmetry of the D and A units in reaching high crystallinity and short π–π stacking distances.[9] Their studies indicate that the centrosymmetric units lead to the straighter backbones, which are more favorable in forming ordered solid-state structures, than the wavy backbones formed by the axisymmetric ones. Bazan and Heeger et al. also reported the significant influences of repeat unit symmetry and main-chain regioregularity in solid-state order and the mobility of OFET devices,[10] and how structural variations affect the molecular dipole moment and phase behaviors.[11] However, when a structural unit of a LBG polymer is modified, accompanied with the symmetrical changes, the strength of the non-covalent interactions among the polymer chains are varied simultaneously, due to the changes in the geometry, orientation and identity of the structural unit.[11] Thus, it remains challenging to clearly differentiate the individual influences from either the symmetrical or the interaction factors of the structural units. To unambiguously identify the influences of the strength of non-covalent interactions on the mesoscopic solid-state structures and the macroscopic optoelectronic performances, in this communication, poly{(5,6-difluorobenzo-2,1,3-thiadiazole-4,7-diyl)-alt-(3′,4″-di-(2-octyldodecyl)-2,2′;5′,2″;5″,2‴-quaterthiophene-5,5‴-diyl)} (PTh_4FBT in **Scheme 1**a) was designed and synthesized. Its physical properties, OFET and BHJ PSC performances were studied and compared to those of its non-fluorinated analogue, poly{(benzo-2,1,3-thiadiazole-4,7-diyl)-alt-(2,2′;5′,2″;5″,2‴-quaterthiophene-5,5‴-diyl)} (PTh_4BT in Scheme 1a), which was previously reported as a LBG polymer with high OFET and PSC performances.[3b] Both 5,6-difluorobenzo-2,1,3-thiadiazole (FBT)[3a] and its non-fluorinated analogue, 2,1,3-benzothiadiazole (BT), are representative of axisymmetrical acceptor units. Replacing the hydrogen atoms at the 5,6- positions of BT with the high electronegativity atoms, fluorine, neither affects the symmetry, nor imposes significantly additional steric hindrance.[3a] This molecular engineering thus excludes the symmetrical factor. More importantly, it enhances the strength of non-covalent interactions among polymer chains, as indicated from our theoretical calculation (Scheme 1b) and experimental results. The stronger non-covalent interaction facilitates the formation of highly ordered solid-state structure and results in higher device performances. Three-dimensional (3D) ordered solid-state structure with long correlation length along the lamellar structure (in the direction along *a* axis), and π–π stacking direction (the direction of *b* axis) were observed from the X-ray diffraction (XRD) experiments. In addition, periodicity along the chain direction (the direction of *c*-axis) was also observed for the first time in the BT based LBG copolymers. The formation of the 3D ordered structure strongly correlates with the excellent optoelectronic performances. PTh_4FBT demonstrates a hole mobility of 0.29 $cm^2V^{-1}s^{-1}$ with I_{on}/I_{off}

Prof. C.-S. Hsu, Prof. C.-L. Wang, J.-F. Jheng, Y.-Y. Lai, J.-S. Wu, Y.-H. Chao
Department of Applied Chemistry
National Chiao Tung University
1001Ta Hsueh Rd., Hsinchu, Taiwan 30010
E-mail: cshsu@mail.nctu.edu.tw; kclwang@nctu.edu.tw

DOI: 10.1002/adma.201300098

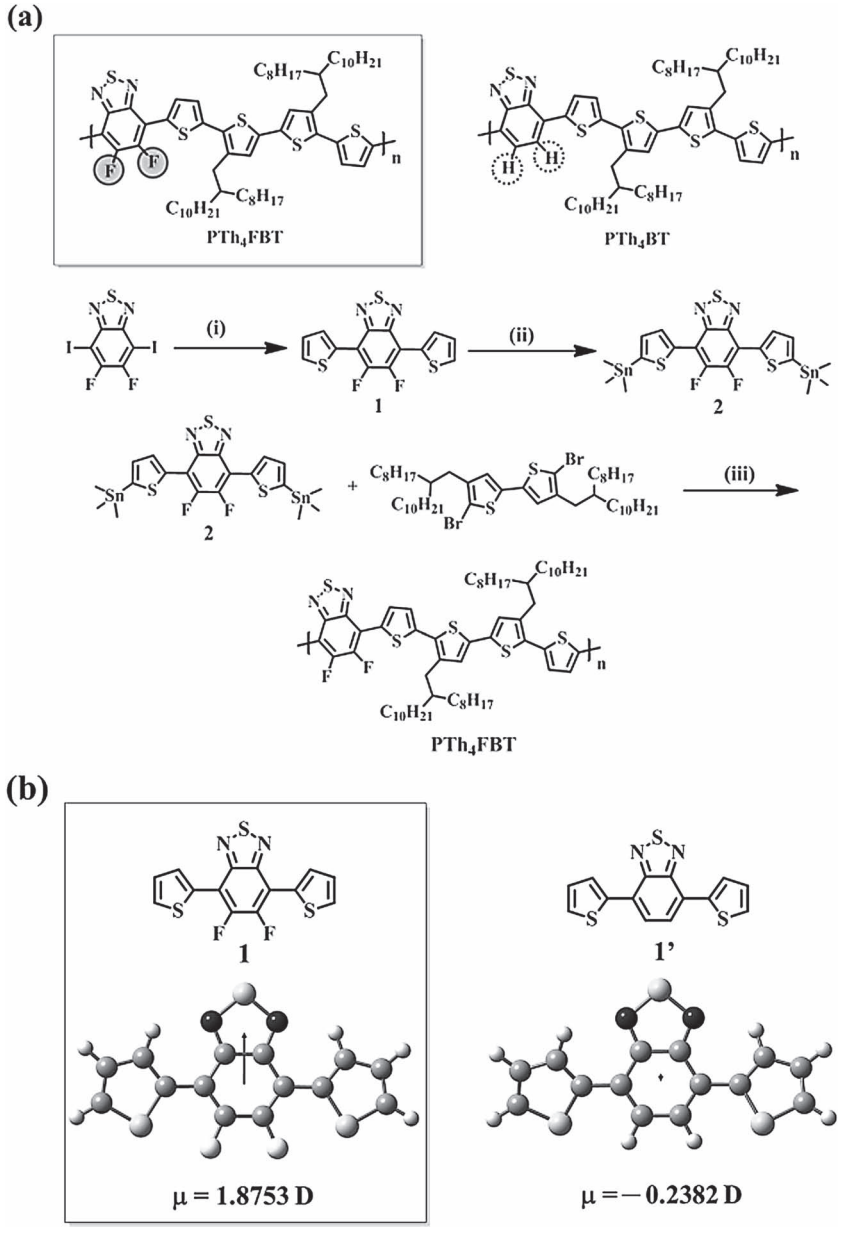

Scheme 1. (a) Chemical structures of PTh_4FBT and PTh_4BT; and synthetic procedure of PTh_4FBT. Reagents and conditions: (i) 2-(tributylstannyl)thiophene, Bis(triphenylphosphine) palladium(II) dichloride, THF, 70 °C, 12 hr; (ii) LDA, dry THF, −78 °C, 1 hr; 1 M trimethyltin chloride; (iii) tris(dibenzylideneacetone)dipalladium(0), tri(o-tolyl)phosphine, chlorobenzene, 180 °C, microwave 270 W, 50min. (b) Illustration of dipole moment of 1 and 1'. The arrow indicates the direction of the dipole moment. The length of the arrow is decided by the strength of the dipole moment. The unit of the dipole moment is given in Debye and the direction is denoted by the arithmetic sign.

ratio of 5.13×10^7 and PCEs of 6.41% and 6.82% in the normal and inverted BHJ PSCs, respectively.

The synthetic route of PTh_4FBT is shown in Scheme 1a. The Stille-coupling reaction between FBT with 2-(tributylstannyl) thiophene was employed to afford the formation of 5,6-difluoro-4,7-di(thiophen-2-yl)benzo-2,1,3-thiadiazole (**1**) in good yield (76%). Lithiation of **1** with lithium diisopropylamide (LDA) followed by reacting with trimethyltin chloride afforded nearly quantitative formation of 5,6-difluoro-4,7-bis(5-(trimethylstannyl)thiophen-2-yl)benzo-2,1,3-thiadiazole (**2**). PTh_4FBT was obtained as black solid via microwave-assisted Stille-coupling copolymerization between **2** and 5,5′-dibromo-4,4′-bis(2-octyldodecyl)-2,2′-bithiophene. Long and branched 2-octyldodecyl side chains were adopted to ensure adequate solubility of the polymer.[3b] The polymer is soluble in warm chlorinated benzenes, slightly soluble in chloroform, but has poor solubility in tetrahydrofuran (THF). The molecular weight of PTh_4FBT was not obtainable from GPC measurement due to its poor solubility in THF. PTh_4FBT exhibited good thermal stability with decomposition temperature (T_d) of 416 °C measured by thermogravimetric analysis (Figure S1). In the differential scanning calorimetry (DSC) analysis as shown in Figure S2, an endothermic transition at 270 °C (ΔH = 10.76 J/g) during heating and an exothermic transition at 257 °C (ΔH = 10.84 J/g) during cooling were observed. The nearly identical latent heats during the cooling and heating scans indicates that PTh_4FBT exhibits an enantiotropic phase behavior and possess a thermodynamically stable ordered solid-state structure in the temperature region below 270 °C. Furthermore, the melting point of PTh_4BT was reported in the literature as 213 °C.[12] The much higher transition temperatures of PTh_4FBT indicate the increased difficulty in disrupting crystallinity, and suggest a stronger intermolecular non-covalent interactions brought by the FBT unit.

The absorption spectra for PTh_4FBT in *o*-dichlorobenzne (ODCB) solution and thin film are shown in **Figure 1**. The absorption bands with λ_{max}s around 400 nm and at 575 nm band can be attributed to localized π–π* transition, and intramolecular charge transfer (ICT) between the electron-rich quaterthiophene units and the electron-deficient FBT units, respectively. Both absorption bands bathochromically shift when PTh_4FBT was spin-casted into thin film. Furthermore, the low-energy absorption shoulder at 690 nm shows a stronger absorption intensity in the thin film, implying the stronger π–π interactions and better coplanarity of the polymer chains in the solid-state.[13] Notably, the shoulder peak at 690 nm remained even at a solution temperature of 100 °C. Compared to the UV-vis spectra of PTh_4BT,[3b] where the low-energy absorption shoulder completely disappears at a ODCB solution temperature of 45 °C, the higher difficulty to dis-aggregate PTh_4FBT in the ODCB solution thus also supports the stronger non-covalent interactions among PTh_4FBT. The optical bandgap (E_g) was deduced to be 1.65 eV from the

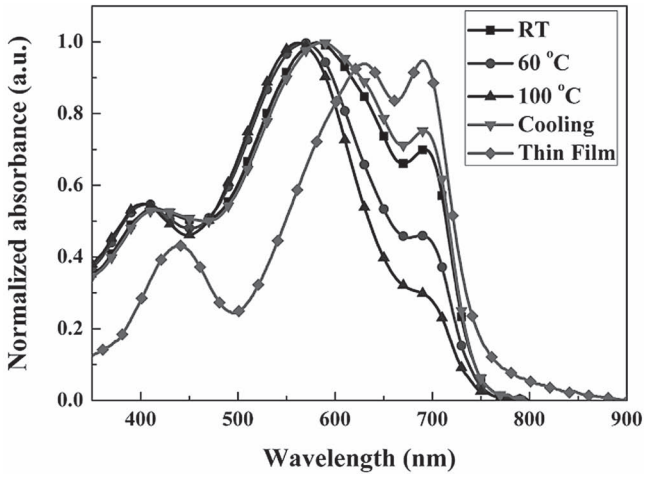

Figure 1. Normalized UV-vis absorption spectra of PTh_4FBT in ODCB solution at different temperatures and in the thin film.

absorption edge of the thin film spectrum. Figure S3 shows the cyclic voltammetry (CV) measurements of PTh_4FBT. The E_{HOMO} and E_{LUMO} of PTh_4FBT were determined to be −5.54 eV and −3.68 eV based on their onset redox potentials. The low-lying E_{HOMO} of PTh_4FBT is expected to impart good air stability in OFET applications and a high V_{oc} in BHJ PSCs.

Figure 2 shows the in-situ X-ray powder diffraction pattern of PTh_4FBT. The diffraction peaks located at the scattering vector (q) = 3.00, 6.00, 9.00 and 12.0 (nm^{-1}) can be indexed as (100), (200), (300) and (400) diffractions. Appearance of the high ordered peaks indicate the presence of long-range ordered lamellar structure with d-spacing of 2.09 nm. In addition, the strong (010) diffraction located at q = 16.8 (nm^{-1}) suggests the ordered π–π stacking with d-spacing of 0.37 nm. The ordered

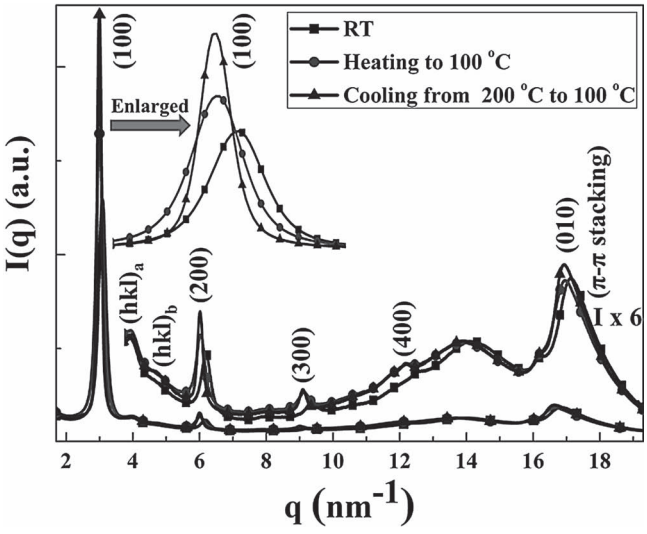

Figure 2. In-situ X-ray powder diffraction patterns of PTh_4FBT at different temperatures. The insets are the enlarged patterns, which clearly show that after cooled from 200 °C, the sample has stronger and narrower diffraction peaks.

lamellar structure of PTh_4BT has recently been reported by de Mello and Chen et al.[12] However, unlike PTh_4FBT, which develops long-range ordered lamellar structure and π–π stacking before thermal treatment, ordered lamellar structure of PTh_4BT formed only after thermal annealing at 200 °C. Moreover, ordered π–π stacking was not observed in PTh_4BT even after the thermal treatment. Since the 5,6-difluoro substitution on the BT unit is the only molecular difference between PTh_4FBT and PTh_4BT, the improvements in the solid-state order can be unambiguously attributed to the stronger intermolecular non-covalent interactions induced by the FBT units.

To gain insight into the intrinsic disparity between the BT and FBT units, theoretical calculations were performed with the Gaussian09[14] suite employing the WB97XD density functional in combination with the 6-311G(d,p) basis set. **1** and **1′** were used as simplified models for PTh_4FBT and PTh_4BT, respectively. The optimized structures and the calculated dipole moments are illustrated in Scheme 1b. It is evident that the substitution of hydrogen by fluorine on the 5,6-positions of BT unit results in a dramatic change in the molecular dipole moment. Heeger and co-workers have pointed out that self-assembly could be driven by the orientation and strength of the molecular dipole moment.[11b] One can therefore hypothesize that the change of the molecular dipole moment from BT to FBT results in a different intermolecular packing manner. Furthermore, it has been demonstrated experimentally and computationally that substituents, such as fluorine, on the aromatic rings are advantageous to the π–π stacking.[15] Therefore, the replacement of BT by FBT can not only change the molecular dipole moment, but also promote the intermolecular interaction, which enhanced the order of π–π stacking.

Table 1 lists the correlation lengths (L_{hkl}) of the lamellar structure (L_{100}) and π–π stacking (L_{010}) deduced based on the full width at half-maximum of the diffraction peaks using the Scherrer equation.[16] L_{hkl} represents the length scale of the periodicity of a set of (hkl) planes to be preserved. The as-precipitated sample already shows significantly long L_{100} of 22.7 nm and L_{010} of 5.8 nm, indicating the highly crystalline nature of PTh_4FBT. Further increases in crystallinity and L_{hkl} was achieved by heating the sample to 200 °C and then cooled. The L_{100} and L_{010} further increased to 38.8 nm and to 6.0 nm, respectively. The in-situ X-ray diffraction clearly demonstrates the increases in the intensity and sharpness of the (100) and (010) diffractions (the insets of Figure 2). The degree of solid-state structural order shows good correlation with the mobilities of the PTh_4FBT based OFET devices, as shown later. Moreover, two additional diffraction peaks ($(hkl)_a$ and $(hkl)_b$ in Figure 2) were also observed. These peaks do not belong to any (hk0)

Table 1. Averaged correlation lengths, L_{100} and L_{010}, of PTh_4FBT deduced from the in situ X-ray powder diffraction.

	L_{100} [nm] (for the lamellar structure)	L_{010} [nm] (for the π–π stacking)
As-precipitated	22.7	5.8
Heated to 100 °C	23.6	5.8
Cooled from 200 to 100 °C	38.8	6.0

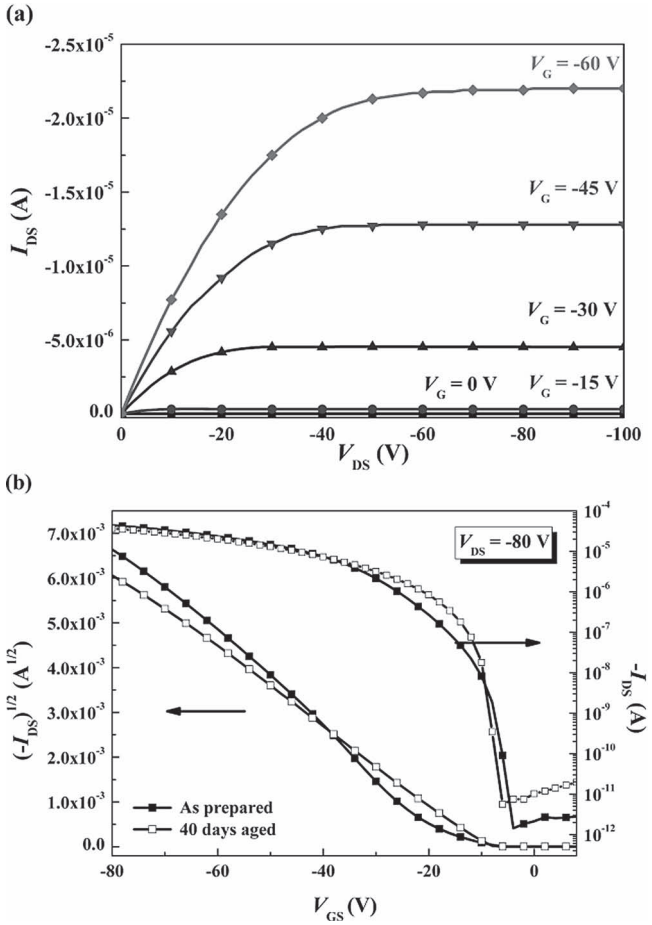

Figure 3. (a) Output curves of the OFET devices base on PTh_4FBT and (b) transfer plots displaying the saturated regime for the as-prepared and aged devices.

diffraction, because of their large *d*-spacings (1.57 and 1.33 nm), and thus implies the presence of periodical structure along the chain direction (*c*-axis). It is likely that through enhancing the inter-chain non-covalent interactions, not only the ordered lamellar and π–π stackings, but also the periodicity along the chain direction can be induced. Detailed structural characterization of PTh_4FBT is currently under investigated and will be published elsewhere.

To investigate the charge transport properties of PTh_4FBT, OFET devices using a bottom-gate, top-contact configuration with evaporated gold as source and drain electrodes were prepared. The SiO_2 gate dielectric on *n*-doped silicon wafer surface was treated with a self-assembled monolayer (SAM) of octadecyltrichlorosilane (ODTS). The output and transfer plots of the devices exhibited typical *p*-channel OFET characteristics (**Figure 3**). As shown in **Table 2**, The OFET device annealed at 200 °C showed one order of magnitude higher mobility than the one annealed at 100 °C. The results correlate well with the X-ray diffraction experiments (Figure 2 and Table 1), which showed higher crystallinity and longer L_{100} and L_{010} for the sample cooled from 200 °C. The hole mobility of the device annealed at 200 °C was 0.29 $cm^2V^{-1}s^{-1}$ with I_{on}/I_{off} ratio of 5.13×10^7.

Table 2. OFET Characteristics of PTh_4FBT. The OFETs are in bottom-gate, top-contact configureation with channel width (*W*) of 1 mm, channel length (*L*) of 0.1 mm, and PTh_4FBT thickness of 60 nm.

Annealing Temp. [°C]	Mobility [$cm^2V^{-1}s^{-1}$]	I_{on}/I_{off}	V_{th} [V]
100	2.91×10^{-2}	1.44×10^7	−20.9
200	2.89×10^{-1}	5.13×10^7	−18.4

The improved solid-state order and L_{hkl} thus enabled PTh_4FBT to reach the highest mobility among the BT-quarterthiophene based alternating copolymers.[3b,8a] Because of its low E_{HOMO}, preliminary stability tests also showed the air stability of the device. After exposed in air without encapsulation for 40 days, the mobility maintained at 0.15 $cm^2V^{-1}s^{-1}$.

To evaluate the photovoltaic performances of PTh_4FBT, BHJ PSCs with conventional architecture–indium tin oxide (ITO)/PEDOT:PSS (40 nm)/PTh_4FBT:$PC_{71}BM$ (95 nm)/Ca (35 nm)/Al (100 nm) and inverted architecture - ITO/ZnO (30 nm)/PTh_4FBT:$PC_{71}BM$ (95 nm)/MoO_3 (6 nm)/Ag (150 nm) were prepared. Their performances were measured under 100 mW/cm^2 AM 1.5 illumination. The characterization data are summarized in **Table 3**. The current density-voltage characteristics and incident-photon to current conversion efficiency (IPCE) of these devices are shown in **Figure 4**. The conventional device using PTh_4FBT:$PC_{71}BM$ (1:1, w/w) blend as active layer exhibited a V_{oc} of 0.78 V, a J_{sc} of 12.17 mA/cm^2, a FF of 67.5%, delivering a PCE of 6.41%. The inverted device using identical active layer exhibited a V_{oc} of 0.77 V, a J_{sc} of 13.51 mA/cm^2, a FF of 65.6%, delivering the highest PCE of 6.82% among the BT-quarterthiophene based alternating copolymers.[3b,8a] PTh_4FBT based PSCs provide higher V_{oc} than its non-fluorinated counterpart because of its lower-lying E_{HOMO} caused by the electron-pulling F substituents. The IPCE curve in Figure 4b indicates that the PTh_4FBT:$PC_{71}BM$ active layer provides high photon-to-current conversion across a wide visible spectrum region (350-750nm). The photo-to-electron conversion is more efficient in the inverted device. Over 50% of IPCE was observed from 400 to 710 nm, resulting in the high J_{sc}. Therefore, the lower-lying E_{HOMO} and improved solid-state order enabled PTh_4FBT to reach higher V_{oc} and J_{sc}, and the highest PCE of 6.82% among the BT-quarterthiophene based alternating copolymers.

In conclusion, a novel LBG polymer, PTh_4FBT, which demonstrated the highest OFET mobility (0.29 $cm^2V^{-1}s^{-1}$) and BHJ PSC performances (PCE of 6.82% in inverted PSCs) among the BT-quarterthiophene based alternating copolymer is reported. This LBG polymer showed improved solid-state order resulting in enhanced device performances. Since our molecular engineering excluded the symmetrical factor, the enhancements in the microscopic phase structure and macroscopic device performance can be clearly attributed to the stronger intermolecular non-covalent interactions induced from the F substituents. Our study thus reveals the importance of the strength of non-covalent interaction in reaching high-performance LBG polymer, and promotes a more comprehensive consideration for the polymer design in the future.

Table 3. PSCs Characteristics of $PTh_4FBT:PC_{71}BM$ based BHJ PSCs.

Architecture	$PTh_4FBT:PC_{71}BM$ (weight ratio)	V_{oc} [V]	J_{sc} [mA/cm^2]	FF [%]	PCE [%]
Conventional	1: 1	0.78	12.17	67.5	6.41
Inverted	1: 1	0.77	13.51	65.6	6.82

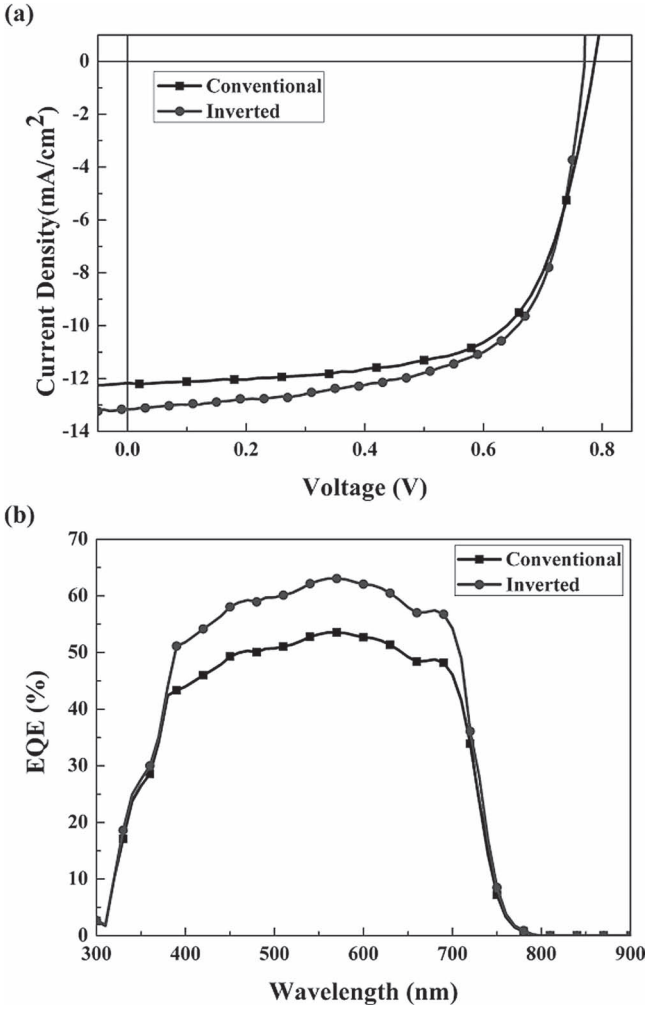

Figure 4. (a) Current density-voltage characteristics and (b) IPCE spectra of $PTh_4FBT:PC_{71}BM$ based BHJ PSCs in the conventional (square symbols) and inverted (circle symbols) device architectures under illumination of AM 1.5 G at 100 mW/cm^2.

Experimental Section

General Measurement and Characterization: All chemicals are purchased from Aldrich, Lancaster, TCI or Acros used as received unless otherwise specified. 5,6-difluoro-4,7-diiodobenzo-2,1,3-thiadiazole[3a] and 5,5'-dibromo-4,4'-bis(2-octyldodecyl)-2,2'-bithiophene[3b] was synthesized according to literature. ^{1}H and ^{13}C NMR spectra were measured using a Varian 300 MHz and 400 MHz instrument spectrometer. Differential scanning calorimeter (DSC) was measured on a TA Q200 Instrument and thermogravimetric analysis (TGA) was recorded on a Perkin Elmer Pyris under nitrogen atmosphere at a heating rate of 10 °C/min. Absorption spectra were collected on a HP8453 UV-vis spectrophotometer. The electrochemical cyclic voltammetry (CV) was conducted on a CH Instruments Model 611D. A Carbon glass coated with a thin polymer film was used as the working electrode and Ag/Ag^+ electrode as the reference electrode, while 0.1 M tetrabutylammonium hexafluorophosphate (Bu_4NPF_6) in acetonitrile was the electrolyte. CV curves were calibrated using ferrocence as the standard, whose oxidation potential is set at –4.8 eV with respect to zero vacuum level. The E_{HOMO} were deduced from the equation $E_{HOMO} = -(E_{ox}^{onset} - E_{(ferrocene)}^{onset} + 4.8)$ eV. The E_{LUMO} levels of polymer were deduced from the equation $E_{LUMO} = -(E_{red}^{onset} - E_{(ferrocene)}^{onset} + 4.8)$ eV.

In-Situ X-ray Powder Diffraction of PTh_4FBT: The powder X-ray diffraction patterns of PTh_4BFT were recorded at the BL01C2 beamline of the National Synchrotron Radiation Research Center (NSRRC) in Taiwan. The ring energy of NSRRC was operated at 1.5 GeV with a typical current of 300 mA. The wavelength of the incident X-rays was 1.0332A° (12.0 keV), delivered from the superconducting wavelength-shifting magnet, and a Si(111) double-crystal monochromator. The diffraction patterns were recorded at room temperature with a Mar345 imaging plate detector approximately 300 mm from sample positions and typical exposure duration 5 minutes. The pixel size of Mar345 was 100 µm. The one-dimensional powder diffraction profile was converted with program FIT2D and cake-type integration. The diffraction angles were calibrated according to Bragg positions of Ag-Benhenate and Si powder (NBS640b) standards. In situ synchrotron X-ray powder diffraction for PTh_4FBT and were performed at BL01C2 from 28 to 200 °C with a heating rate approximately 10 °C/min. The powder sample was sealed in a capillary (1.0 mm diameter) and heated in a stream of hot air; each in situ powder XRD pattern was exposed for about 1.2 minutes. The correlation length (L_{hkl}) were deduced using Sherrer's equation, $L_{hkl} = 0.9\lambda/(\beta_{hkl}\cos\theta)$, where λ is the X-ray wavelength, β_{hkl} is the full width at half maximum of an (hkl) diffraction in radian, and is the θ Bragg diffraction angle.

Computational Details: Quantum–chemical calculations were performed with the Gaussian09 suite[14] employing the WB97XD density functional in combination with the 6–311G(d,p) basis set. Geometry optimizations were performed with tight SCF and convergence criteria and an ultrafine integration grid by applying the GEDIIS optimization algorithm. The minimum nature of each stationary point was confirmed by a frequency analysis.

OFET Device Fabrication and Characterization: An *n*-type heavily doped Si wafer with a SiO_2 layer of 300 nm and a capacitance of 11 nF/cm^2 was used as the gate electrode and dielectric layer. Thin films (40–60 nm in thickness) of polymers were deposited on ODTS treated SiO_2/Si substrates by spin-coating their ODCB solution (5 mg/mL). The thin films were annealed at 100 or 200 °C for 10 minutes. Gold source and drain contacts (40 nm in thickness) were deposited by vacuum evaporation on the organic layer through a shadow mask, affording a bottom-gate, top-contact OFET device. Electrical measurements of the OFET devices were carried out at room temperature in air using a 4156C Semiconductor Parameter Analyzers, Agilent Technologies. The field-effect mobility was calculated in the saturation regime by using the equation, $I_{ds} = (\mu WC_i/2L)(V_g - V_t)^2$, where I_{ds} is the drain-source current, μ is the field-effect mobility, W is the channel width (1 mm), L is the channel length (0.1 mm), C_i is the capacitance per unit area of the gate dielectric layer, V_g is the gate voltage and V_t is threshold voltage.

BHJ PSC Fabrication and Characterization: The device structures for the conventional PSCs was ITO/PEDOT:PSS/$PTh_4FBT:PC_{71}BM$/Ca/Al, and ITO/ZnO/$PTh_4FBT:PC_{71}BM/MoO_3$/Ag for the inverted PSCs. The ITO glass substrates were cleaned with detergent, deionized water, acetone, and isopropyl alcohol in an ultrasonic bath and then dried overnight in

an oven at >100 °C. In conventional PSCs, substrates were covered by PEDOT:PSS (40 nm; Al 4083 provided by H. C. Stark) using spin-coating, and dried in glove box at 150 °C for 30 minutes. PTh_4FBT were dissolved in ODCB (0.4 wt%), and $PC_{71}BM$ (purchased from Nano-C) was then added into the solution to reach the desired weight ratio. The solution was stirred at 70 °C for overnight and filtrated through a 0.45 μm filter. In a glove box, the polymer solution was kept at 120 °C, and then spin-coated at 900 rpm. The devices were solvent annealed with ODCB for 30 minutes, and then annealed at 100 °C for 15 minutes. The cathode made of calcium (35 nm) and aluminum (100 nm) was evaporated through a shadow mask under vacuum (<10^{-6} Torr). For the inverted PSCs, zinc acetylacetonate hydrate (purchased from Aldrich) dissolved in methanol (20 mg mL^{-1}) was spin-casted on pre-cleaned ITO substrates and baked at 130 °C for 10 minutes in the air to form the ZnO layer with thickness of 30 nm. The active layer was spin-casted on the ZnO layer using the identical procedure mentioned above. The anode made of MoO_3 (6 nm) and Ag (150 nm) was evaporated through a shadow mask under vacuum (<10^{-6} Torr). Each sample consists of four independent pixels defined by an active area of 0.04 cm^2. The devices were encapsulated and characterized in air under 100 mW/cm^2 AM 1.5 simulated light measurement (Yamashita Denso solar simulator). Current–voltage (*J–V*) characteristics of PSC devices were obtained by a Keithley 2400 SMU. Solar illumination conforming the JIS Class AAA was provided by a SAN-EI 300W solar simulator equipped with an AM 1.5G filter. The light intensity was calibrated with a Hamamatsu S1336-5BK silicon photodiode.

Synthesis of 5,6-difluoro-4,7-di(thiophen-2-yl)benzo-2,1,3-thiadiazole (**1**): To a round bottom flask was added 5,6-difluoro-4,7-diiodobenzo-2,1,3-thiadiazole (0.5 g, 1.15 mmol), degassed THF (20 mL) and $PdCl_2(PPh_3)_2$ (73 mg, 0.104 mmol). The solution was stirred at 60 °C until all the substance completely dissolved. 2-(tributylstannyl)thiophene (1 g, 2.68 mmol) was added dropwise and the mixture was kept at 60 °C for 20 h. After cooling to room temperature, the mixture solution was poured into a 500 mL flask with ethanol to give the product as an orange solid. Whisker crystals were obtained by recrystallization from methanol. Yield: 300 mg (75.6%). ^{1}H NMR ($CDCl_3$, 300 MHz, δ): 7. 28 (d, J = 4.5 Hz, 2 H), 7.63 (d, J = 5.1 Hz, 2 H), 8.30 (d, J = 3.6 Hz, 2 H); ^{13}C NMR ($CDCl_3$, 75 MHz, δ): 111.91, 127.58, 129.02, 129.06, 131.01, 131.06, 131.12, 131.67, 148.10, 148.36, 149.04, 151.55, 151.83; Anal. calcd for $C_{14}H_6F_2N_2S_3$: C 49.98, H 1.8, N 8.33; found: C 49.97, H 2.12, N 8.20.

Synthesis of 5,6-difluoro-4,7-bis(5-(trimethylstannyl)thiophen-2-yl)benzo-2,1,3-thiadiazole (**2**): To a solution of compound **1** (300 mg, 0.89 mmol) in dry THF (50 mL) was added a 2 M solution of lithium diisopropylamide in THF (1.16 mL, 2.32 mmol) dropwise at −78 °C. After stirring at −78 °C for 1 h, 1.0 M solution of chlorotrimethylstannane in THF (2.32 mL, 2.32 mmol) was introduced by syringe to the solution. The mixture solution was warmed up to room temperature and stirred for 20 h. The mixture solution was extracted with diethyl ether (50 mL × 3) and water (50 mL). Solvent was evaporated under reduced pressure and the product was obtained by recrystallization from methanol. Yield: 573 mg (97%). ^{1}H NMR ($CDCl_3$, 400MHz, δ): 0.45 (s, 18H), 7.36 (d, J = 3.6 Hz, 2 H), 8.35 (d, J = 3.6 Hz, 2H); Anal. calcd for $C_{20}H_{22}F_2N_2S_3Sn_2$: C 36.29, H 3.35, N 4.23; found: C 36.60, H 3.58, N 4.57.

Synthesis of PTh_4FBT: To a 50 mL round bottom flask was added 5,5′-dibromo-4,4′-bis(2-octyldodecyl)-2,2′-bithiophene (114 mg, 0.129 mmol), compound **2** (85.3 mg, 0.129 mmol), tris(dibenzylideneacetone) dipalladium (5.9 mg, 0.05 mmol), tri(2-methylphenyl)phosphine (15.7 mg, 0.4 mmol) and deoxygenated chlorobenzene (5 mL). The mixture was then degassed by bubbling nitrogen for 10 minutes at room temperature. The round bottom flask was put into the microwave reactor and heated to 180 °C under 270 watt for 50 minutes. Then, tributyl(thiophen-2-yl) stannane (10.5 mg, 0.028 mmol) was added to the mixture solution and reacted for 10 minutes under 270 W. Finally, 2-bromothiophene (20 mg, 0.123 mmol) was added to the mixture solution and reacted for 10 minutes under 270 W. After cooling to room temperature the solution was added dropwise to methanol. The precipitate was collected by filtration and washed by Soxhlet extraction with acetone (24 h), hexane (24 h) and tetrahydrofuran (24 h) sequentially. The residue solid was re-dissolved in hot ODCB (100 mL). The Pd-thiol gel (Silicycle Inc.) was added to above ODCB solution to remove the residual Pd catalyst at 100 °C for 12 h. After filtration of solution and removal of the solvent under reduced pressure, the polymer solution was added into methanol to re-precipitate. The purified polymer was collected by filtration and dried under vacuum for 1 day to give a black solid. Yield: 100 mg (50.2%). ^{1}H NMR ($CDCl_3$, 400MHz, δ): 0.45 (br, 12H), 1.26 (br, 64H), 2.67-2.79 (br, 4H), 6.99-7.12 (br, 4H), 8.29 (br, 2H).

Supporting Information

Supporting Information is available from the Wiley Online Library or from the author.

Acknowledgements

This work is supported by the National Science Council and "ATP" of the National Chiao Tung University and Ministry of Education, Taiwan. The authors thank Dr. Hwo-Shuenn Sheu and Dr. U-Ser Jeng at BL01C and BL23A beamlines of the National Synchrotron Radiation Research Center (NSRRC) in Taiwan for assistance with the XRD measurements.

Received: January 7, 2013
Published online: March 1, 2013

[1] a) B. C. Thompson, J. M. J. Fréchet, *Angew. Chem., Int. Ed.* **2008**, *47*, 58; b) Y. Liang, L. Yu, *Acc. Chem. Res.* **2010**, *43*, 1227; c) Y. J. Cheng, S. H. Yang, C. S. Hsu, *Chem. Rev.* **2009**, *109*, 5868; d) Y. F. Li, *Acc. Chem. Res.* **2012**, *45*, 723; e) J. W. Chen, Y. Cao, *Acc. Chem. Res.* **2009**, *42*, 1709; f) A. C. Arias, J. D. MacKenzie, I. McCulloch, J. Rivnay, A. Salleo, *Chem. Rev.* **2010**, *110*, 3; g) C. Duan, F. Huang, Y. Cao, *J. Mater. Chem.* **2012**, *22*, 10416; h) H. Zhou, L. Yang, W. You, *Macromolecules* **2012**, *45*, 607; i) F. He, L. Yu, *J. Phys. Chem. Lett.* **2011**, *2*, 3102; j) G. Li, R. Zhu, Y. Yang, *Nat. Photo.* **2012**, *6*, 153; k) S. Günes, H. Neugebauer, N. S. Sariciftci, *Chem. Rev.* **2007**, *107*, 1324; l) C. Wang, H. Dong, W. Hu, Y. Liu, D. Zhu, *Chem. Rev.* **2012**, *112*, 2208; m) I. McCulloch, R. S. Ashraf, L. H. Bronstein, C. Combe, J. E. Donaghey, D. I. James, C. B. Nielsen, B. C. Schroeder, W. Zhang, *Acc. Chem. Res.* **2012**, *45*, 714; n) Y. G. Wen, Y. Q. Liu, Y. L. Guo, G. Yu, W. P. Hu, *Chem. Rev.* **2011**, *111*, 3358; o) P. M. Beaujuge, J. M. J. Fréchet, *J. Am. Chem. Soc.* **2011**, *133*, 20009; p) A. R. Murphy, J. M. Fréchet, *Chem. Rev.* **2007**, *107*, 1066.

[2] a) M. C. Scharber, D. Wuhlbacher, M. Koppe, P. Denk, C. Waldauf, A. J. Heeger, C. L. Brabec, *Adv. Mater.* **2006**, *18*, 789; b) M. M. Wienk, M. Turbiez, J. Gilot, R. A. J. Janssen, *Adv. Mater.* **2008**, *20*, 2556.

[3] a) H. Zhou, L. Yang, A. C. Stuart, S. C. Price, S. Liu, W. You, *Angew. Chem. Int. Ed.* **2011**, *50*, 2995; b) K.-H. Ong, S.-L. Lim, H.-S. Tan, H.-K. Wong, J. Li, Z. Ma, L. C. H. Moh, S.-H. Lim, J. C. de Mello, Z.-K. Chen, *Adv. Mater.* **2011**, *23*, 1409; c) C. M. Amb, S. Chen, K. R. Graham, J. Subbiah, C. E. Small, F. So, J. R. Reynolds, *J. Am. Chem. Soc.* **2011**, *133*, 10062; d) Y. Sun, C. J. Takacs, S. R. Cowan, J. H. Seo, X. Gong, A. Roy, A. J. Heeger, *Adv. Mater.* **2011**, *23*, 2226; e) Q. Peng, X. J. Liu, D. Su, G. W. Fu, J. Xu, L. Dai, *Adv. Mater.* **2011**, *23*, 4554; f) C. Y. Chang, Y. J. Cheng, S. H. Hung, J. S. Wu, W. S. Kao, C. H. Lee, C. S. Hsu, *Adv. Mater.* **2012**, *24*, 549; g) H. J. Son, W. Wang, T. Xu, Y. Liang, Y. Wu, G. Li, L. Yu, *J. Am. Chem. Soc.* **2011**, *133*, 1885; h) S. C. Price, A. C. Stuart, L. Yang, H. Zhou, W. You, *J. Am. Chem. Soc.* **2011**, *133*, 4625; i) K. Takimiya, S. Shinamura, I. Osaka, E. Miyazaki, *Adv. Mater.* **2011**, *23*, 4347.

[4] a) Z. He, C. Zhong, X. Huang, W.-Y. Wong, H. Wu, L. Chen, S. Su, Y. Cao, *Adv. Mater.* **2011**, *23*, 4636; b) Y. J. Cheng, C. H. Hsieh, Y. He,

C. S. Hsu, Y. Li, *J. Am. Chem. Soc.* **2010**, *132*, 17381; c) C. Y. Chang, C. E. Wu, S. Y. Chen, C. Cui, Y. J. Cheng, C. S. Hsu, Y. L. Wang, Y. Li, *Angew. Chem. Int. Ed.* **2011**, *50*, 9386; d) L. Dou, J. You, J. Yang, C. C. Chen, Y. He, S. Murase, T. Moriarty, K. Emery, G. Li, Y. Yang, *Nat. Photon.* **2012**, *6*, 180; e) C. E. Small, S. Chen, J. Subbiah, C. M. Amb, S.-W. Tsang, T. H. Lai, J. R. Reynolds, F. So, *Nat. Photon.* **2012**, *6*, 115.

[5] a) Z. Chen, M. J. Lee, R. Shahid Ashraf, Y. Gu, S. Albert-Seifried, M. M. Nielsen, B. Schroeder, T. D. Anthopoulos, M. Heeney, I. McCulloch, H. Sirringhaus, *Adv. Mater.* **2012**, *24*, 647; b) H. Bronstein, Z. Chen, R. S. Ashraf, W. Zhang, J. Du, J. R. Durrant, P. S. Tuladhar, K. Song, S. E. Watkins, Y. Geerts, M. M. Wienk, R. A. J. Janssen, T. Anthopoulos, H. Sirringhaus, M. Heeney, I. McCulloch, *J. Am. Chem. Soc.* **2011**, *133*, 3272; c) H. N. Tsao, D. M. Cho, I. Park, M. R. Hansen, A. Mavrinskiy, D. Y. Yoon, R. Graf, W. Pisula, H. W. Spiess, K. Müllen, *J. Am. Chem. Soc.* **2011**, *133*, 2605; d) H. J. Chen, Y. L. Guo, G. Yu, Y. Zhao, J. Zhang, D. Gao, H. T. Liu, Y. Q. Liu, *Adv. Mater.* **2012**, *24*, 4618; e) D. H. Kim, B. L. Lee, H. Moon, H. M. Kang, E. J. Jeong, J. I. Park, K. M. Han, S. Lee, B. W. Yoo, B. W. Koo, J. Y. Kim, W. H. Lee, K. Cho, H. A. Becerril, Z. Bao, *J. Am. Chem. Soc.* **2009**, *131*, 6124; f) X. Guo, R. P. Ortiz, Y. Zheng, M.-G. Kim, S. Zhang, Y. Hu, G. Lu, A. Facchetti, T. J. Marks, *J. Am. Chem. Soc.* **2011**, *133*, 13685; g) T. Lei, Y. Cao, Y. L. Fan, C. J. Liu, S. C. Yuan, J. Pei, *J. Am. Chem. Soc.* **2011**, *133*, 6099; h) J. G. Mei, D. H. Kim, A. L. Ayzner, M. F. Toney, Z. N. Bao, *J. Am. Chem. Soc.* **2011**, *133*, 20130.

[6] a) J.-M. Lehn, *Proc. Natl. Acad. Sci. USA* **2002**, *99*, 4763; b) G.M. Whitesides, J.P. Mathias, C.T. Seto, *Science* **1991**, *254*, 1312; c) L. Brunsveld, J. A. J. M. Vekemans, J. H. K. K. Hirschberg, R. P. Sijbesma, E. W. Meijer, *Proc. Natl. Acad. Sci. USA* **2002**, *99*, 4977; d) S. Leininger, B. Olenyuk, P. J. Stang, *Chem. Rev.* **2000**, *100*, 853; e) D. Philp, J. F. Stoddart, *Angew. Chem. Int. Ed.* **1996**, *35*, 1154.

[7] a) J. Peet, J. Y. Kim, N. E. Coates, W. L. Ma, D. Moses, A. J. Heeger, G. C. Bazan, *Nat. Mater.* **2007**, *6*, 497; b) J. K. Lee, W. L. Ma, C. J. Brabec, J. Yuen, J. S. Moon, J. Y. Kim, K. Lee, G. C. Bazan, A. J. Heeger, *J. Am. Chem. Soc.* **2008**, *130*, 3619; c) W. Ma, C. Yang, X. Gong, K. Lee, A. J. Heeger, *Adv. Funct. Mater.* **2005**, *15*, 1617; d) T. Erb, U. Zhokhavets, G. Gobsch, S. Raleva, B. Stuhn, P. Schilinsky, C. Waldauf, C. J. Brabec, *Adv. Funct. Mater.* **2005**, *15*, 1193; e) A. T. Yiu, P. M. Beaujuge, O. P. Lee, C. H. Woo, M. F. Toney, J. M. J. Frechet, *J. Am. Chem. Soc.* **2012**, *134*, 2180.

[8] a) I. Osaka, M. Shimawaki, H. Mori, I. Doi, E. Miyazaki, T. Koganezawa, K. Takimiya, *J. Am. Chem. Soc.* **2012**, *134*, 3498; b) A. T. Yiu, P. M. Beaujuge, O. P. Lee, C. H. Woo, M. F. Toney, J. M. J. Fréchet, *J. Am. Chem. Soc.* **2011**, *134*, 2180; c) E. G. Wang, Z. F. Ma, K. Vandewal, P. Henriksson, O. Inganäs, F. L. Zhang, R. A. Andersson, *J. Am. Chem. Soc.* **2011**, *133*, 14244; d) E. Wang, L. Hou, Z. Wang, S. Hellström, F. Zhang, O. Inganäs, M. R. Andersson, *Adv. Mater.* **2010**, *22*, 5240; e) M. S. Su, C. Y. Kuo, M. C. Yuan, U. S. Jeng, C. J. Su, K. H. Wei, *Adv. Mater.* **2011**, *23*, 3315; f) C. H. Chen, Y. J. Cheng, C. Y. Chang, C. S. Hsu, *Macromolecules* **2011**, *44*, 8415; g) Y. J. Cheng, C. H. Chen, Y. S. Lin, C. Y. Chang, C. S. Hsu, *Chem. Mater.* **2011**, *23*, 5068; h) Y. J. Cheng, S. W. Cheng, C. Y. Chang, W. S. Kao, M. H. Liao, C. S. Hsu, *Chem. Commun.* **2012**, *48*, 3203; i) J. S. Wu, Y. J. Cheng, T. Y. Lin, C. Y. Chang, P. I. Shih, C. S. Hsu, *Adv. Funct. Mater.* **2012**, *22*, 1711; j) J. S. Wu, C. T. Lin, C. L. Wang, Y. J. Cheng, C. S. Hsu, *Chem. Mater.* **2012**, *24*, 2391.

[9] a) S. Shinamura, I. Osaka, E. Miyazaki, A. Nakao, M. Yamagishi, J. Takeya, K. Takimiya, *J. Am. Chem. Soc.* **2011**, *133*, 5024; b) T. Lei, Y. Cao, X. Zhou, Y. Peng, J. Bian, J. Pei, *Chem. Mater.* **2012**, *24*, 1762; c) T. Lei, J.-H. Dou, J. Pei, *Adv. Mater.* Article ASAP, DOI: 10.1002/adma201202689.

[10] L. Ying, B. B. Y. Hsu, H. M. Zhan, G. C. Welch, P. Zalar, L. A. Perez, E. J. Kramer, T.-Q. Nguyen, A. J. Heeger, W.-Y. Wong, G. C. Bazan, *J. Am. Chem. Soc.* **2011**, *133*, 18538.

[11] a) Z. B. Henson, G. C. Welch, T. van der Poll, G. C. Bazan, *J. Am. Chem. Soc.* **2012**, *134*, 3766; b) C. J. Takacs, Y. Sun, G. C. Welch, L. A. Perez, X. Liu, W. Wen, G. C. Bazan, A. J. Heeger, *J. Am. Chem. Soc.* **2012**, *134*, 16597.

[12] K.-H. Ong, S.-L. Lim, J. Li, H.-K. Wong, H.-S. Tan, T. T. Lin, L. C. H. Moh, J. C. de Mello, Z.-K. Chen, *Polym. Chem.* **2012** Article ASAP, DOI: 10.1039/C2PY20898A.

[13] C. Yang, F. P. Orfino, S. Holdcroft, *Macromolecules* **1996**, *29*, 6510.

[14] M. J. Frisch, G. W. Trucks, H. B. Schlegel, G. E. Scuseria, M. A. Robb, J. R. Cheeseman, G. Scalmani, V. Barone, B. Mennucci, G. A. Petersson, H. Nakatsuji, M. Caricato, X. Li, H. P. Hratchian, A. F. Izmaylov, J. Bloino, G. Zheng, J. L. Sonnenberg, M. Hada, M. Ehara, K. Toyota, R. Fukuda, J. Hasegawa, M. Ishida, T. Nakajima, Y. Honda, O. Kitao, H. Nakai, T. Vreven, Jr., J. A. Montgomery, J. E. Peralta, F. Ogliaro, M. Bearpark, J. J. Heyd, E. Brothers, K. N. Kudin, V. N. Staroverov, R. Kobayashi, J. Normand, K. Raghavachari, A. Rendell, J. C. Burant, S. S. Iyengar, J. Tomasi, M. Cossi, N. Rega, J. M. Millam, M. Klene, J. E. Knox, J. B. Cross, V. Bakken, C. Adamo, J. Jaramillo, R. Gomperts, R. E. Stratmann, O. Yazyev, A. J. Austin, R. Cammi, C. Pomelli, J. W. Ochterski, R. L. Martin, K. Morokuma, V. G. Zakrzewski, G. A. Voth, P. Salvador, J. J. Dannenberg, S. Dapprich, A. D. Daniels, Ö. Farkas, J. B. Foresman, J. V. Ortiz, J. Cioslowski, D. J. Fox, Gaussian 09, Revision A.1; Gaussian, Inc., Wallingford CT, **2009**.

[15] a) C. D. Sherrill, *Acc. Chem. Res.* **2012**, Article ASAP, DOI: 10.1021/ar3001124; b) S. E. Wheeler, *Acc. Chem. Res.* **2012**, Article ASAP, DOI: 10.1021/ar300109n.

[16] a) A. T. Yiu, P. M. Beaujuge, O. P. Lee, C. H. Woo, M. F. Toney, J. M. J. Fréchet, *J. Am. Chem. Soc.* **2011**, *134*, 2180; b) T. Erb, U. Zhokhavets, G. Gobsch, S. Raleva, B. Stuhn, P. Schilinsky, C. Waldauf, C. J. Brabec, *Adv. Funct. Mater.* **2005**, *15*, 1193.